Electrophysiological and morphological characteristics of three subtypes of rat globus pallidus neurone *in vitro*

A. J. Cooper and I. M Stanford

Department of Pharmacology, Division of Neuroscience, The Medical School, University of Birmingham, Edgbaston, Birmingham B15 2TT, UK

(Received 7 April 2000; accepted after revision 19 June 2000)

1. Neurones of the globus pallidus (GP) have been classified into three subgroups based on the visual inspection of current clamp electrophysiological properties and morphology of biocytin-filled neurones.

2. Type A neurones (132/208; 63 %) were identified by the presence of the time- and voltage-dependent inward rectifier (I_h) and the low-threshold calcium current (I_t) giving rise to anodal break depolarisations. These cells were quiescent or fired regular spontaneous action potentials followed by biphasic AHPs. Current injection evoked regular activity up to maximum firing frequency of 350 Hz followed by moderate spike frequency adaptation. The somata of type A cells were variable in shape (20×12 μm) while their dendrites were highly varicose.

3. Type B neurones (66/208; 32 %) exhibited neither I_h nor rebound depolarisations and only a fast monophasic AHP. These cells were spontaneously active while current injection induced irregular patterns of action potential firing up to a frequency of 440 Hz with weak spike frequency adaptation. Morphologically, these cells were the smallest encountered (15×10 μm), oval in shape with restricted varicose dendritic arborisations.

4. Type C neurones were much rarer (10/208; 5 %). They were identified by the absence of I_h and rebound depolarisations, but did possess a prolonged biphasic AHP. They displayed large A-like potassium currents and ramp-like depolarisations in response to step current injections, which induced firing up to a maximum firing frequency of 310 Hz. These cells were the largest observed (27×15 μm) with extensive dendritic branching.

5. These results confirm neuronal heterogeneity in the adult rodent GP. The driven activity and population percentage of the three subtypes correlates well with the *in vivo* studies (Kita & Kitai, 1991). Type A cells appear to correspond to type II neurones of Nambu & Llinas (1994, 1997) while the small diameter type B cells display morphological similarities with those described by Millhouse (1986). The rarely encountered type C cells may well be large cholinergic neurones. These findings provide a cellular basis for the study of intercellular communication and network interactions in the adult rat *in vitro*.

The globus pallidus (GP) of the rat (equivalent to the external segment of the GP in primates) is becoming increasingly thought of as the central integrator of basal ganglia neurotransmission (Parent & Hazrati, 1995). It is composed of a network of inhibitory GABA-containing projection neurones which relays information derived from the striatum not only to the excitatory neurones of the subthalamic nucleus (STN) (Smith *et al.* 1990; Parent & Hazrati, 1995) but also to the internal segment of the globus pallidus (GP_i) (Kincaid *et al.* 1991; Bolam & Smith, 1992), substantia nigra pars reticulata (SNr) (Smith & Bolam, 1989), reticular thalamic nucleus (Cornwall *et al.* 1990; Hazrati & Parent, 1991; Gandia *et al.* 1993) and striatum (Bevan *et al.* 1998).

In accordance with its central role in basal ganglia circuitry, changes in the activity of the GP are apparent in disorders of movement. In 1-methyl-4-phenyl-1,2,3,6-tetrahydropyridine (MPTP) models of Parkinson's disease, neuronal GP firing shows a greater propensity to burst firing with increased synchronisation (Filion & Tremblay, 1991; Nini *et al.* 1995) while neuronal bursting activity in the GP has been correlated with muscle tremor (Bergman *et al.* 1998). Indeed, it has recently been proposed that the GP and STN constitute a central pacemaker responsible for oscillatory activity driven by the cortex (Magill *et al.* 2000), that appears to be under the control of intact inhibitory dopamine inputs (Plenz *et al.* 1999).

As a prerequisite to the study of synchronous oscillatory activity and of dopamine pharmacology of this nucleus (see Cooper & Stanford, 2000), a study of GP neuronal heterogeneity was undertaken for comparison with previous literature. The precise classification of GP neuronal subtypes based on their membrane properties and ionic conductances is an essential initial step in understanding their individual role within the GP and basal ganglia network as a whole. Indeed, the intrinsic activity of individual GP cells including firing rate and pattern will depend on the expression of a variety of voltage-dependent channels.

Due to the diverse nature of previous studies in the GP it is difficult to arrive at a clear consensus on GP neuronal heterogeneity. Early extracellular recordings *in vivo* from primates indicated four types of GP firing pattern (Delong, 1971) while early anatomical studies in the rat reported only one major and two rarer GP subtypes (Millhouse, 1986). Recent morphological studies in the rat have revealed two types of projection neurones (Park *et al.* 1992; Kita & Kitai, 1994; Nambu & Llinas, 1997) while electrophysiological studies have revealed three subtypes of GP neurone *in vivo* in the rat (Kita & Kitai, 1991) and *in vitro* in the guinea-pig (Nambu & Llinás, 1994) using sharp microelectrode recordings.

Here, we combine whole-cell electrophysiology with the morphological characterisation of GP neurones visualised in a slice prepared from adult rats. To our knowledge this is the first whole-cell study in the GP, a technique which allows recordings from cells throughout the whole structure including the more fibrous ventro-medial GP and from somata whose size and shape are not conducive to sharp electrode placement. The whole-cell mode also avoids the electrode shunting of small conductance, thus providing a more accurate assessment of ionic conductance, which are small in amplitude. Using this technique we have found evidence for three subtypes of GP neurone in the adult rat. Thus, in this study, we present: (a) whole-cell electrophysiological characterisation of three types of rat GP neurones, (b) the morphology of electrophysiologically classified neurones and (c) the topographical distribution of the different classes.

METHODS

In vitro slice preparation

Thick slices (300 μm) of GP–striatum were obtained from 80–120 g male Wistar rats as previously outlined (Stanford & Cooper, 1999). Briefly, animals were first anaesthetised with fluorothane (4% in O_2) and killed by cervical dislocation in accordance with the Animals (Scientific Procedures) Act, 1986, UK. The brain was quickly removed and placed in ice cold artificial cerebral spinal fluid (aCSF) containing (mM): choline chloride 126, KCl 2·5, NaH_2PO_4 1·2, $MgCl_2$ 1·3, $MgSO_4$ 8, glucose 10, buffered to pH 7·4 with $NaHCO_3$ (26 mM). Slices were cut in either the coronal or parasagittal plane using a DTK-1000 Microslicer (Dosaka, Japan). The slices were then transferred to a holding chamber or recording chamber at 32–34 °C where they were perfused continuously at 2–3 ml min^{-1} with aCSF containing (mM): NaCl 126, KCl 2·5, NaH_2PO_4 1·2, $MgCl_2$ 1·3, $CaCl_2$ 2·4, glucose 10, buffered to pH 7·4 with $NaHCO_3$ (26 mM) saturated with 95% O_2–5% CO_2.

Electrophysiological recording

Whole-cell recordings were made using borosilicate glass pipettes of 3–6 MΩ resistance containing (mM): potassium gluconate 125, NaCl 10, $CaCl_2$ 1, $MgCl_2$ 2, BAPTA 10, Hepes 10, GTP 0·3, Mg-ATP 2, biocytin 5, adjusted to pH 7·25 with KOH. Individual neurones were visualised (× 40 water immersion objective) using differential interference contrast infa-red microscopy (Olympus BX 501, Japan) with CCD camera (Hitachi KP-M1, Japan) and contrast enhancement system (ADV-2, Brian Reece Scientific Ltd, Newbury, UK). GP cells were selected solely on the basis of apparent neuronal viability and were not consciously selected on the basis of somata size or shape. Recording pipettes were advanced while under positive pressure towards individual cells in the slice. On contact, tight seals, in the order of 10–20 GΩ, were made by applying negative pressure. The membrane patch was then ruptured by suction and membrane current and potential were monitored using an Axopatch 200B patch clamp amplifier (Axon Instruments, Foster City, CA, USA). Whole-cell access resistances were in the range 7–20 MΩ prior to electrical compensation by 65–80%. Access resistance, following electrical compensation, was initially determined in current-clamp mode and continuously monitored in voltage-clamp mode, by measuring the size of the capacitance transient in response to a 10 mV hyperpolarising step (Stuart *et al.* 1993). The access resistance was checked intermittently in current-clamp mode and experiments were abandoned if changes > 20% were encountered. All current-clamp recordings were made in Axopatch 200B fast mode and membrane potentials were corrected for the liquid junction potentials, estimated to be +8 mV and to the null potential measured at the end of recording.

Drugs were applied to the superfusate by exchanging the aCSF for a solution differing only by the addition of a known concentration of drug, with a dead time of approximately 20 s. Drugs used were tetraethyl-ammonium chloride (TEA-Cl), CsCl and $NiCl_2$ (all from Sigma, UK), tetrodotoxin (TTX, Alomone Laboratories, Israel) and 4-ethylphenylamino-1,2-dimethyl-6-methylaminopyrimidinium chloride (ZD 72888, Tocris Cookson Ltd, UK).

Biocytin histochemistry

Pipette biocytin (Sigma, UK) was injected via alternate ± 0·5 nA pulses 150 ms in duration at 1 Hz for a period in excess of 20 min. The attached pipette was then carefully removed from the bath and the slice left for > 2 h for the diffusion of biocytin to distal neuronal elements. Slices were fixed in 4% paraformaldehyde in 0·1 M phosphate buffer (PBS) at 4 °C until processed. Biocytin-filled neurones were revealed in the whole mount using a modified method involving avidin–biotin complex (Elite ABC kit, Vector Laboratories). After washing in 0·1 M PBS, slices were incubated with 0·3% H_2O_2 for 30 min to block endogenous peroxidase activity. Following further washes in PBS and 0·1% BSA the slices were incubated in sodium borohydride (in 1% in PBS) for 5 min. Permeabilisation in 0·3% Triton X-100 in PBS was followed by incubation with avidin–biotin complex at 4 °C overnight. Further washes in PBS were followed by reaction with 3,3′-diamino-benzidine tetrahydrochloride (0·025% DAB), 0·35% ammonium nickel sulphate and 0·0006% H_2O_2 in Tris-HCl, pH 7·4, under visual inspection for 10–40 min. Slices were rinsed and mounted onto gelatine-coated slides. After overnight drying they were dehydrated in ethanol, cleared in xylene and mounted in the xylene-based mountant (Eukitt). Stained neurones were visualised with the light microscope and drawn with a camera lucida. The

location of each cell was mapped onto a stylised drawing of GP slices (after Paxinos & Watson, 1986).

All numerical data are expressed as means and standard error of the mean unless otherwise stated. One way ANOVAs followed by Tukeys *post hoc* test was used to assess statistical significant differences in the membrane and morphological characteristics of the four neuronal GP subtypes.

Some of these results have been presented in abstract form (Stanford & Cooper, 2000).

RESULTS

Whole-cell patch clamp recordings were made from 296 GP neurones. Neurones were considered viable if resting membrane potential (voltage when steady-state current = 0) < -40 mV (prior to junction potential correction), input resistance > 100 MΩ and action potential amplitude > 50 mV. Neurones that did not meet these criteria were discarded.

For all 296 cells recorded in the GP, frequency distribution histograms of resting membrane potential (measured in voltage clamp at $I = 0$) (Fig. 1*A*); input resistance (1/input conductance measured in response to 10 mV hyperpolarising step from −60 mV) (Fig. 1*B*) and action potential duration (taken as the time between the point of initiation of the maximum rate of depolarisation and the equipotential point during spike repolarisation) (Fig. 1*C*) were plotted.

The frequency distributions for each of these parameters did not follow a normal distribution. The distribution of resting membrane potentials (RMP) shows at least two peaks (at RMP of −65 and −56 mV) and a skew to less negative potentials (Fig. 1*A*). Input resistance and action potential duration were also both skewed towards lower values, indicative of a heterogeneous population of GP neurones.

The recorded cells (208) were classified into three subgroups based on visual inspection of current-clamp properties including the presence of the anomalous inward rectifier I_h, anodal break rebound depolarisations and the presence of monophasic or biphasic after-hyperpolarisations (AHPs) (see Table 1). Classifying cells in this way (by qualitative means) avoids the biasing of numerical data. Cells remained unclassified (75 in total) if they did not fully conform to the criteria outlined in Table 1. We acknowledge that within these 75 cells, there may be further GP subtypes, which were not identified. However, there appears to be no difference in the distribution of resting membrane potential, input resistance or action potential duration in these unclassified cells (shown in Fig. 1, open bars) to those whose phenotype has been determined (Fig. 1, filled bars), indicating that a large sub-population of GP neurones, with significantly different resting membrane potential, input resistance or action potential duration, has not been overlooked.

Table 1. GP neurones were classified on the basis of visual assessment of current clamp data

Cell type	I_h	Rebound depolarisations	Biphasic AHP	Spontaneous activity
A	+	+	+	−/+
B	−	−	−	+
C	−	−	+	−

Three groups of cells were found to meet these four criteria fully. Neurones, which differed in one or more of these properties, remained unclassified.

Of the remaining 13 cells, 11 were identified as non-GP neurones on the basis of location (of biocytin fills) and by comparison with previous studies. These cells included medium spiny striatal neurones, cholinergic interneurones

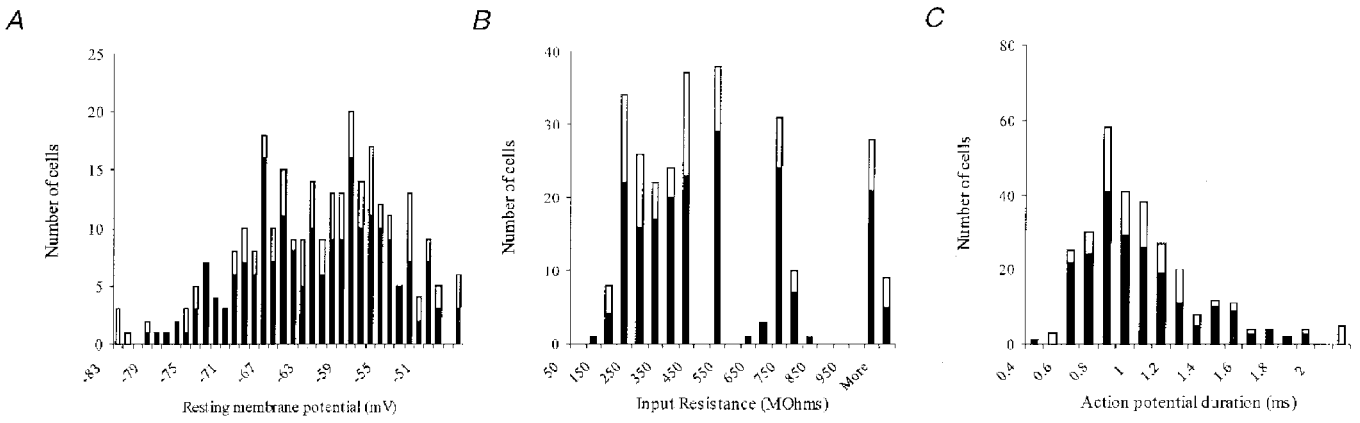

Figure 1. Frequency distribution histograms of membrane characteristics are indicative of a heterogeneous population of GP neurones

Of 296 cells recorded in the GP 208 (70%) have been classified into three subtypes (filled bars). Open bars indicate unclassified cells. Frequency distribution histograms of resting membrane potential (*A*), input resistance (*B*) and action potential duration (*C*). None of these parameters exhibited a Gaussian distribution expected of a homogenous population of neurones indicative of two or more cell types in the GP.

of the striatum, and neurones in ventral portions of the slice with characteristics of ventral pallidal neurones. Two other cells of fusiform somata were found on the striatal/GP border. It is unclear at present whether these constitute a fourth GP neuronal subtype.

Type A neurones

Of the classifiable GP cells 132/208 (63%) were classed as type A neurones. They were easily identified by the presence of a time- and voltage-dependent 'sag' of membrane potential evoked by hyperpolarising current steps and anodal break rebound depolarisations, which were often accompanied by action potential firing (Fig. 2*A*).

Significant membrane characteristics of type A neurones include their activity, which was either quiescent (54%) or fired regular spontaneous action potentials at a rate of $7{\cdot}6 \pm 1{\cdot}3$ Hz, at a resting membrane potential of $-66{\cdot}3 \pm 0{\cdot}8$ mV. Their input resistance was $558{\cdot}9 \pm 30{\cdot}1$ MΩ and action potential duration $1{\cdot}04 \pm 0{\cdot}03$ ms. On depolarisation, these cells also displayed transient and sustained voltage-dependent outward currents (data not shown due to the presence of 'breakthrough' action currents).

The time- and voltage-dependent 'sag' of membrane potential evoked by hyperpolarising steps was investigated in more detail. In voltage clamp, step hyperpolarisations were applied from a holding potential of −60 mV in order to evoke the inward current (Figs 2*C* and 3*A*). A plot of instantaneous current (I_{ins}, measured after 15 ms) and steady-state current (I_{ss}, measured after 135 ms) against voltage, highlights the time-dependent activation of this current at potentials more negative than −70 mV (Fig. 3*A*).

The depolarising 'sag' in membrane voltage (and inward current in voltage clamp) was blocked by bath application of CsCl (2 mM, $n = 3$) or ZD 7288 (100 μM, $n = 4$) (Fig. 3*B* and *C*) showing it to be due to the time- and voltage-dependent anomalous inward rectifier I_h (Harris & Constanti, 1995).

The activation of anodal rebound depolarisations and action potential firing on the termination of hyperpolarising current pulses is most likely due to the presence of a transient, low voltage-activated calcium conductance (I_t). In voltage clamp at a holding potential of −100 mV in the presence of TTX (1 μM) and TEA-Cl (20 mM, to block outward potassium currents), 2·5 mV depolarising steps of 100 ms duration elicited a transient inward current

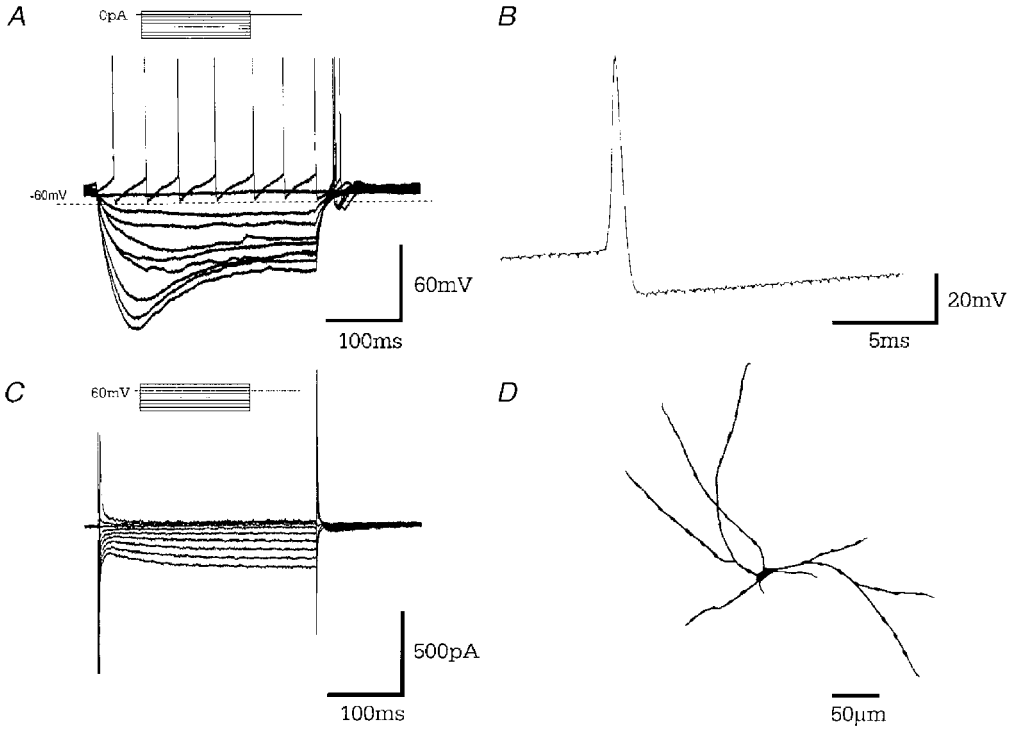

Figure 2. Type A GP neurones

A, records of membrane potential in response to a series of 300 ms current steps (in 25 pA increments) from resting membrane potential. Large hyperpolarising current steps elicit a characteristic time- and voltage-dependent 'sag' in membrane potential. Rebound depolarisations often accompanied by action potential firing were produced on repolarisation of the membrane. *B*, a representative single action potential of duration 1·03 ms followed by long lasting after-hyperpolarisation. *C*, records of membrane current in response to a series of 300 ms steps (10 mV increments) from a holding potential of −60 mV showing time- and voltage-dependent inward current evoked on hyperpolarising voltage steps. *D*, camera lucida drawing of type A multipolar GP neurone with varicose dendrites following intracellular labelling with biocytin.

activated at a potential of $-62{\cdot}5 \pm 3{\cdot}1$ mV, reaching a peak of $310 \pm 53{\cdot}2$ pA at $-52{\cdot}8 \pm 3{\cdot}2$ mV (8 cells). In these conditions, voltage steps to potentials more depolarised than -50 mV still produced an inactivating outward current that curtailed the inward current (Fig. 4*A*).

Bath application of $NiCl_2$ (1 mM, $n = 4$), which exhibits some selectivity for the I_t, abolished the inward current completely while also having a small effect on outward current (Fig. 4*B*). $NiCl_2$ (1 mM) also reversibly blocked rebound spiking by reducing the amplitude of rebound depolarisations (see Fig. 4*C*). The remaining rebound depolarisation is presumably due to the de-inactivation of I_h.

Type B neurones

Type B cells make up 66/208 (32%) of the GP neuronal population classified. These cells showed no evidence of I_h, I_t or rebound depolarisations (Fig. 5*A* and *C*) but did possess the transient (A-like) and sustained outward currents. They were spontaneously active, firing irregular action potentials at $13{\cdot}6 \pm 2{\cdot}4$ Hz, at a resting membrane potential of $-58{\cdot}1 \pm 1{\cdot}1$ mV. Their input resistance was the lowest of all GP subtypes at $311{\cdot}5 \pm 20{\cdot}1$ MΩ, while action potential duration was the shortest at $0{\cdot}73 \pm 0{\cdot}02$ ms (see Table 2). The action potential was followed by a monophasic short lasting AHP of amplitude $26{\cdot}7 \pm 0{\cdot}8$ mV (Fig. 5*B*).

Type C neurones

Type C neurones were much rarer, forming only 10/208 (4·5%) of the GP cells classified. These cells were identified by having neither I_h nor rebound depolarisations. They did exhibit a biphasic AHP and a long membrane time constant of $36{\cdot}5 \pm 4{\cdot}7$ ms, consistent with the largest input resistance of $698{\cdot}2 \pm 221{\cdot}9$ MΩ of the three subtypes of GP neurone (Fig. 6). These neurones were also quiescent at a resting membrane potential of $-66{\cdot}6 \pm 2{\cdot}4$ mV. Action potentials were of long duration ($1{\cdot}11 \pm 0{\cdot}12$ ms) and were followed by a small but prolonged AHP of amplitude $19{\cdot}8 \pm 1{\cdot}8$ mV. In voltage clamp, depolarising current steps from resting membrane potential elicited a large transient outward current indicative of I_A.

The membrane characteristics of all 208 GP cells including statistical comparisons between different neuronal groups A, B and C are given in Table 2.

Response to current injection

To examine the differences in the driven activity in each of the three cell types, responses to step depolarisations of

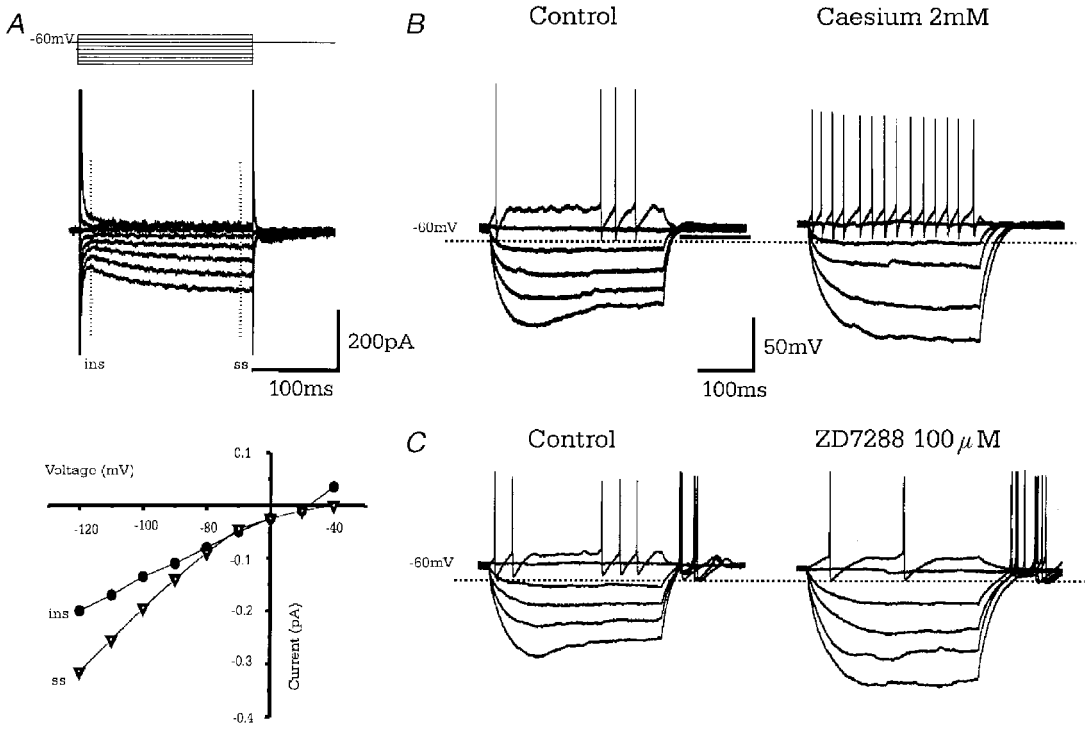

Figure 3. Type A cells show anomalous time- and voltage-dependent inward rectification (I_h)

A, superimposed membrane currents in response to a series of 200 ms voltage steps, in 10 mV increments, from −120 to −40 mV from a holding potential of −60 mV. Hyperpolarising steps evoke a slow time- and voltage-dependent inward current (I_h). The instantaneous current (●, ins) and steady state current (▲, ss) are plotted in current–voltage relationship below showing activation at potentials less than −70 mV. *B*, records of membrane potential in response to a series of current steps showing pronounced sag of membrane voltage due to I_h. Bath application of caesium chloride (2 mM) increases the membrane resistance and abolishes the sag in membrane voltage. *C*, records of membrane potential from a different cell showing that bath application of ZD7288 (100 μM) a specific blocker of I_h also abolishes the sag in membrane voltage.

Table 2. Overview of the membrane properties of GP cells

	RMP (mV)	Input resistance (MΩ)	AP duration (ms)	AP amplitude (mV)	AHP amplitude (mV)	AP threshold (mV)	Membrane time constant (ms)	Firing pattern
Type A $n = 132$	−66·3 ± 0·8	558·9 ± 30·1	1·04 ± 0·03	73·6 ± 1·0	25·5 ± 0·5	−42·1 ± 0·7	25·4 ± 1·0	Quiescent(54%) or regular 7·6 ± 1·3 Hz
Type B $n = 66$	−58·1 ± 1·1	311·5 ± 20·1	0·73 ± 0·02	70·0 ± 1·0	26·7 ± 0·8	−42·9 ± 0·8	19·9 ± 1·6	Irregular 13·6 ± 2·4 Hz
Type C $n = 10$	−66·6 ± 2·4	698·2 ± 222	1·11 ± 0·12	78·8 ± 2·9	19·8 ± 1·8	−42·5 ± 1·9	36·3 ± 4·7	Quiescent
A *vs.* B	0·001	0·001	0·001	n.s.	n.s.	n.s.	0·05	
A *vs.* C	n.s.	n.s.	n.s.	n.s.	0·05	n.s.	0·01	
B *vs.* C	0·01	0·001	0·001	n.s.	0·01	n.s.	0·001	

Values represent means ± S.E.M. Statistical analysis was carried out by one way ANOVAs followed by Tukey's *post hoc* test of significance. The lower three rows show significance between groups. n.s. not significant.

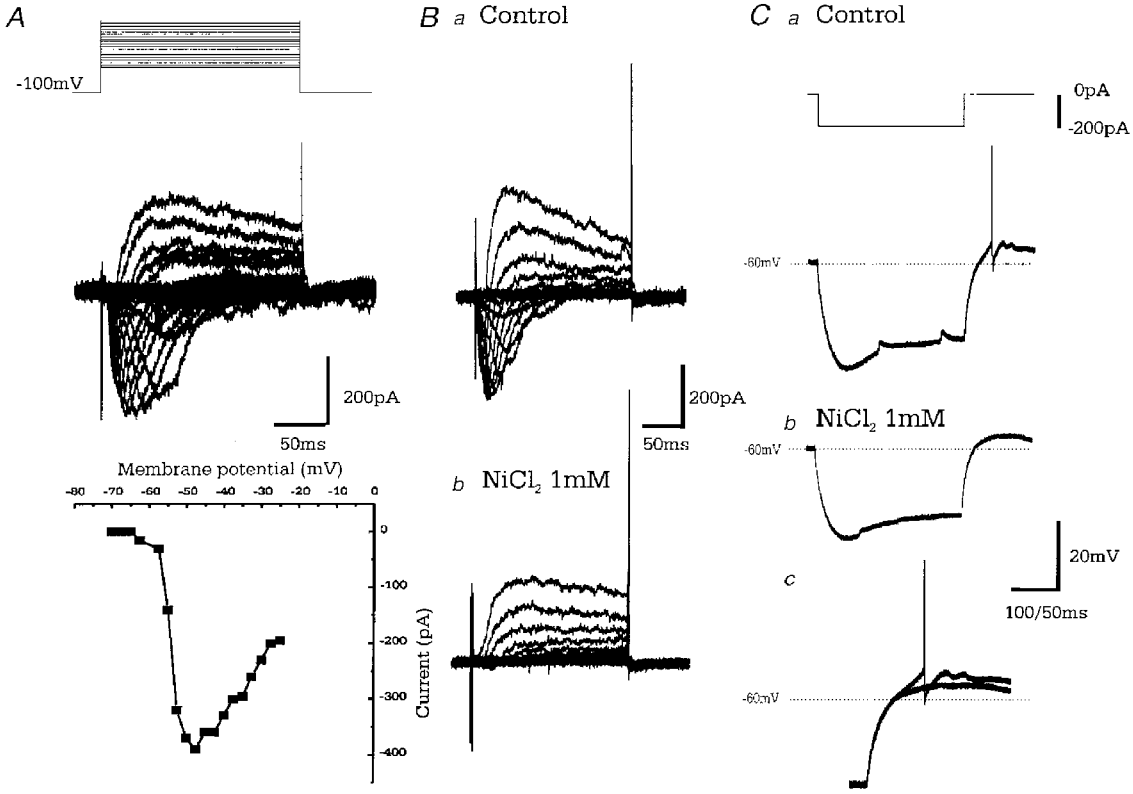

Figure 4. Type A cells have a low threshold calcium conductance (I_t)

A, upper panel: superimposed leak subtracted (P/4) membrane currents from a type A cell in response to voltage steps (increments of 2·5 mV beginning at −70 mV), from a holding potential of −100 mV in the presence of TTX (1 μM) and TEA-Cl (20 mM). Lower panel: current–voltage relationship for the inward currents shows activation at −57·5 mV reaching a peak at −47·5 mV. Residual TEA-Cl insensitive outward currents are evoked at more depolarised step potentials. *B*, leak subtracted (P/4) currents evoked as in *A*, showing control (*a*) and the effect of bath application of $NiCl_2$ (1 mM; *b*). The inward current is abolished, while the outward component also appears reduced by $NiCl_2$ *C*, voltage records in response to 200 pA hyperpolarising steps in control (*a*) and upon bath application of $NiCl_2$ (1 mM; *b*). *Cc* shows a comparison of *a* and *b* highlighting the reduction in amplitude of the rebound depolarisation and abolition of action potential firing.

1000 ms duration were assessed. The pattern of firing, the extent of spike frequency adaptation and the maximum frequency of activity immediately prior to spike accommodation and plateau of membrane potential due to lack of spike repolarisation were examined. Representative cells from each subtype are shown with instantaneous frequency (calculated from inter-spike interval) plotted against time in Fig. 7.

Type A cells show regular firing and moderate spike frequency adaptation, which increased in concert with the amplitude of depolarising current steps. The maximum frequency of firing prior to spike accommodation was $353 \pm 21{\cdot}6$ Hz ($n = 16$). Type B cells show irregular firing often grouped into doublets or triplets. This accounts for the spread of points in the instantaneous frequency plots. Once again there is weak spike frequency adaptation except when in response to very large current steps which ultimately induced spike accommodation. The maximum possible firing rate prior to accommodation was $437 \pm 18{\cdot}6$ Hz ($n = 9$, significantly different from type A cells $P < 0{\cdot}05$). Type C cells show a ramp-like depolarisation in response to current steps, which elicits a steady increase in the frequency of cell firing. This appears to mask any adaptation at low amplitude current steps but may be overcome when large current steps are given to cause spike accommodation. The maximum firing frequency of these cells was $307 \pm 43{\cdot}4$ Hz ($n = 4$, significantly different from type B cells, $P < 0{\cdot}05$).

Cell morphology

Of the 61 cells that were sufficiently well labelled with biocytin to allow morphological reconstruction, 40 were fully characterised electrophysiologically. The shape of their soma was either round–oval, triangular–pyramidal, multipolar or fusiform. The dendritic fill extended beyond 500 μm while in a few cases the fill was truncated in a bulbous nature indicating the cut surface of the slice (see Fig. 8*A*). The majority of dendrites were varicose although smooth dendrites were encountered. At the light microscope level there was no evidence for dendritic spines. Axon visualisation in the whole-cell mount was rare, but when possible, was fine and varicose in nature originating from the soma. Of the 40 biocytin-labelled cells that were electrophysiologically characterised, 26 were type A, 10 type B and 4 type C. These properties are summarised in Table 3.

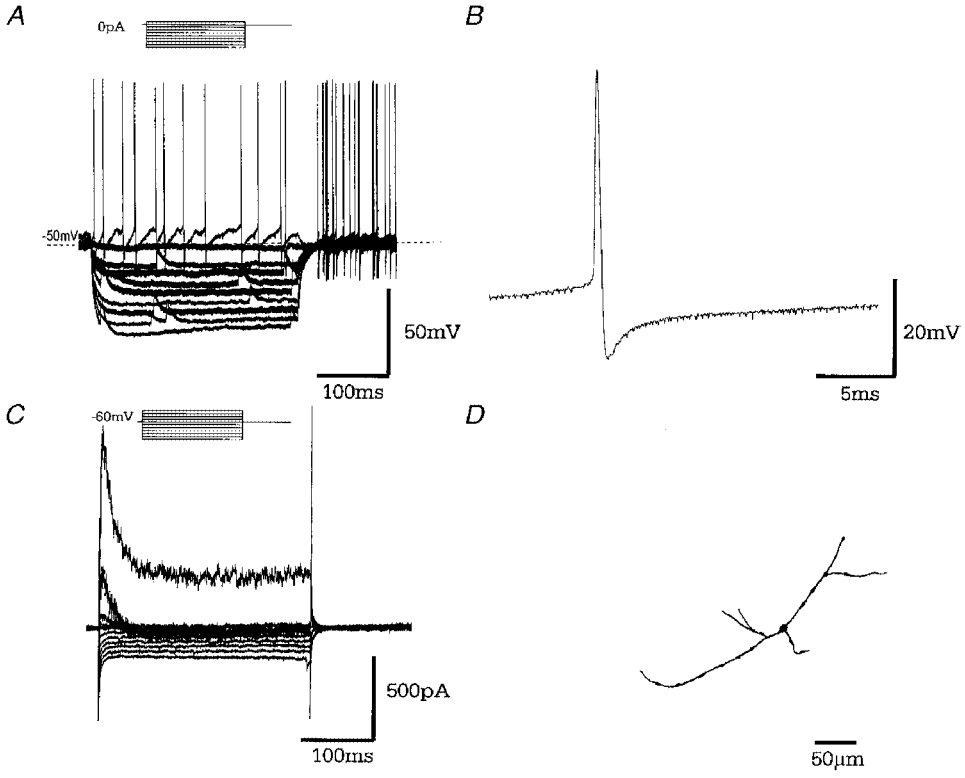

Figure 5. Type B GP neurones

A, records of membrane potential in response to a series of 300 ms hyperpolarising current steps (in 25 pA increments), from resting membrane potential showing no evidence for 'sag' in membrane potential and no rebound depolarisations. Note the spontaneous activity of this cell. *B*, a representative single action potential showing action potential duration of 0·68 ms followed by a short lasting (fast) after-hyperpolarisation. *C*, records of membrane current in response to a series of 300 ms steps (10 mV increments) from a holding potential of −60 mV showing little evidence for I_h. On depolarising steps there is evidence of an inward current and both transient and sustained outward currents. *D*, camera lucida drawings of a typically small type B GP neurone with sparse dendritic tree, following intracellular labelling with biocytin.

Table 3. Light microscope overview of cell morphology

	A $n = 26$	B $n = 10$	C $n = 4$	A *vs.* B	A *vs.* C	B *vs.* C
Shape of soma						
Oval	39%	90%	50%			
Pyramidal	38%	10%	50%			
Other	23%	—	—			
Soma axis (μm)						
Long	19·5 ± 1·5	14·9 ± 1·7	27·3 ± 5·0	0·05	n.s.	0·05
Short	12·3 ± 0·7	10·5 ± 0·3	15·0 ± 2·0	n.s.	n.s.	0·05
No. of primary dendrites	3·4 ± 0·1	3·2 ± 0·2	4·3 ± 0·5	n.s.	n.s.	0·05
No. of secondary dendrites	4·9 ± 0·4	3·6 ± 0·4	7·5 ± 1·0	n.s.	0·05	0·01
Distance to first branching (μm)	17·8 ± 2·5	41·3 ± 10·2	11·9 ± 1·9	0·01	n.s.	0·05
Dendrites						
Varicose	80%	70%	50%			
Smooth	20%	30%	50%			

Values represent means ± S.E.M. Statistical analysis was carried out by one way ANOVAs followed by Tukey's *post hoc* test of significance.

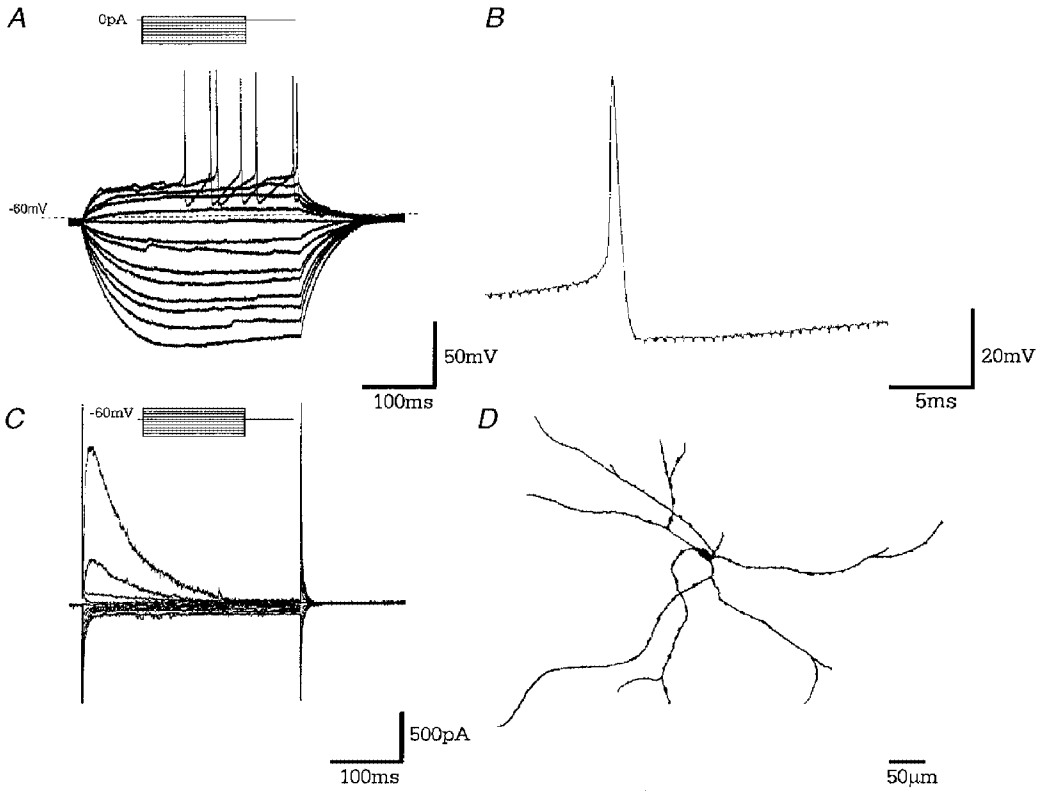

Figure 6. Type C neurones

A, records of membrane potential in response to a series of 300 ms current steps (in 25 pA increments), from resting membrane potential. Note the resting membrane potential of this quiescent cell, long time constant of membrane charging, the lack of I_h and rebound depolarisations. *B*, a representative single action potential showing action potential duration of 0·95 ms followed by a prolonged after-hyperpolarisation. *C*, records of membrane current in response to a series of 300 ms steps (10 mV increments) from a holding potential of −60 mV. There is no evidence of I_h on hyperpolarising voltage steps. A large transient outward current was observed on depolarising steps indicative of I_A. *D*, camera lucida drawings of a typical large pyramidal, type C GP neurone following intracellular labelling with biocytin.

Type A neurones were observed in a variety of somatic shapes including oval, pyramidal and multipolar (see Figs 2*D* and 8*A*). These cells were of medium size (19·5 × 12·3 μm) with extensive dendritic branching, which were mainly varicose (21/26 cells). Type B cells were the smallest encountered (14·9 × 10·5 μm, the long axis dimensions being significantly different from type A and C cells) and mainly oval in shape (Fig. 8*B*). Their dendrites were predominantly varicose (7/10 cells) although did not appear to branch as much as type A neurones as shown by a large distance to the first branching point (41·3 μm, also significantly different from type A and type C cells) and a lower number of primary and secondary dendrites. Type C cells were slightly larger than type A neurones (27 × 15 μm) and were either pyramidal (50%) or oval (50%) in shape. These cells have the largest number of primary dendrites (significantly different from type B neurones) while the extent of secondary dendritic branching was also significantly more than type A or B neurones (see Table 3). The long time constant of membrane charging, which is observed in these cells, is consistent with extensive dendritic arborisation.

Topographic distribution

Direct visualisation of the recorded cell in the slice preparation allows one to record from neurones throughout the GP in coronal and sagittal planes including the ventromedial portions where there are increased numbers of fibre bundles. There appears to be a homogenous distribution of type A, B and C neurones throughout the GP (Fig. 9).

DISCUSSION

Subtyping GP neurones on the basis of current clamp properties

This is the first study addressing the issue of GP heterogeneity using the whole-cell technique. Three types of adult rat GP neurone have been classified on the basis of their electrophysiological and morphological properties. Neurones were initially grouped on the basis of inspection of the current-clamp properties including the presence of the

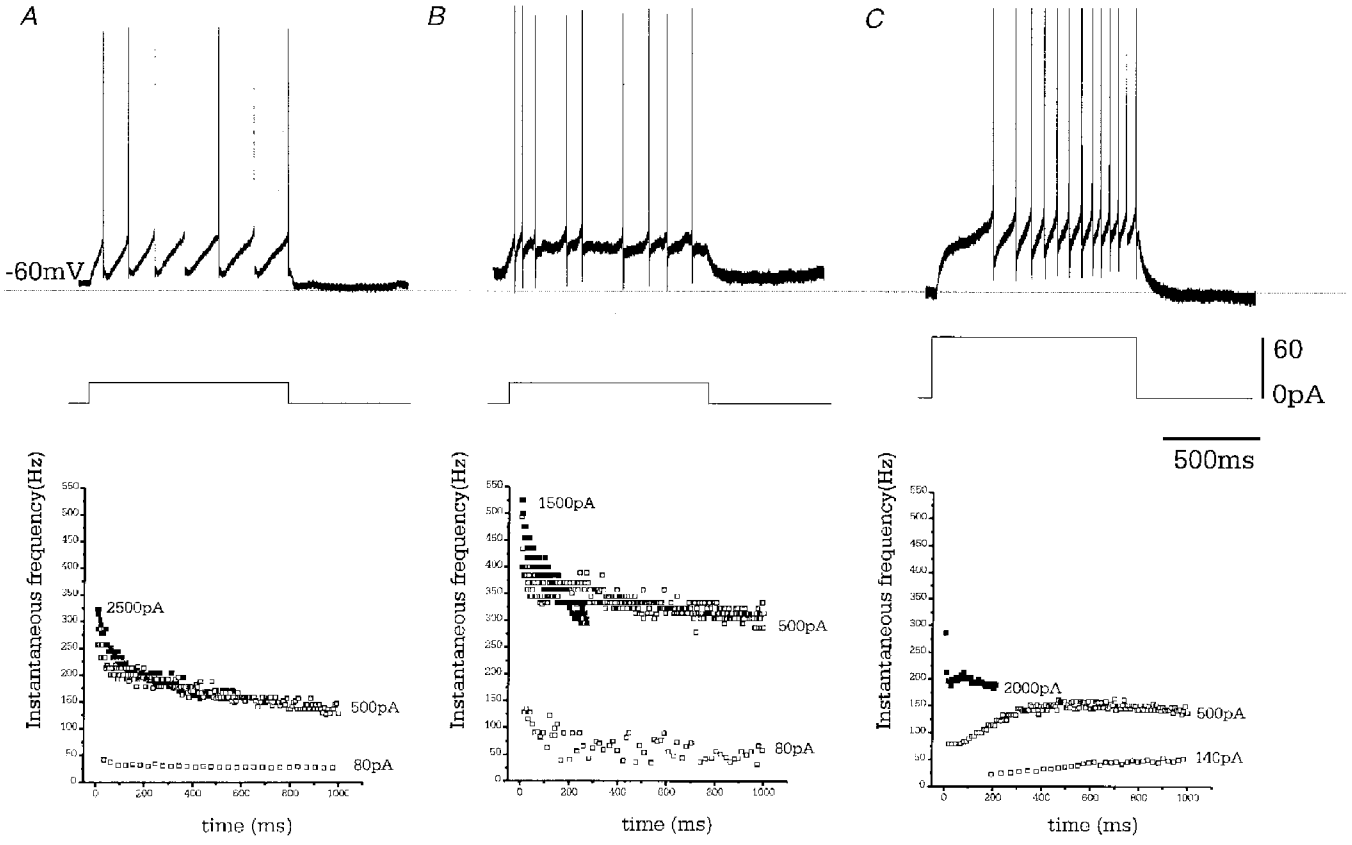

Figure 7. Driven activity of GP cells

Depolarising current steps of 1000 ms duration were applied from resting membrane potential. Representative voltage records are given for each cell type, showing minimal current required to elicit action potential firing. Note the regular firing of type A cell, the irregular firing of type B cells and the ramp-like depolarisation of type C cell. Instantaneous frequencies against time during current step, for a series of step depolarisations are shown below. B-type cells can sustain highest firing frequency although this rate is very irregular. Spike frequency adaptation increases with the size of the current step in both A and B cells. ■, frequency of activity immediately prior to spike accommodation.

time- and voltage-dependent anomalous rectifier (I_h), rebound depolarisations, after-hyperpolarisations and firing rate. Grouping in this way avoids the biasing of subsequent statistical data. The statistical differences in the membrane properties, the presence of transient calcium and potassium currents, responses to current injection and the morphology of biocytin-filled cells provide further support for the classification of cells on the basis of these four qualitative criteria. However, the possibility of further GP neuronal subtypes as yet unidentified remains.

Technical considerations

The relative numbers of cells in each class must be viewed with caution, as there are many reasons why the proportion of cells may differ from other studies. Although the only criteria for choosing cells was apparent cell viability, the size and shape of each cell will be a factor in the success of each recording. Also, those cells with characteristics which are easier to recognise (such as the I_h and rebound depolarisations) may increase the relative proportion of these cells in the characterised GP population.

The frequency of spontaneous action potential firing of neurones of the GP *in vitro* appears to be much lower than that reported *in vivo*, where the incidence of bursting activity is much higher (Delong, 1971; Kita & Kitai, 1991; Magill *et al.* 2000). This makes it difficult to compare subtypes of GP neurone on the basis of firing rate alone and may indicate that activity pattern generation is dependent on functionally intact excitatory synaptic connections. Also, in comparing the neuronal characteristics with those from previous studies one must take into account differences in species, whether it be primate, rat or guinea-pig, the preparation being used and whether extracellular, sharp microelectrode or whole-cell recordings were conducted.

Comparisons of cell types with previous studies

Type A cells. Type A neurones are principally characterised by the presence of I_h and rebound depolarisations. No time- and voltage-dependent anomalous rectification (I_h) has previously been reported in any GP cell population. The proportion of quiescent type A cells (and firing rate of the remaining neurones in this class), action potential spike duration and input resistance (although × 5 larger with the whole-cell patch recordings of the present study) compare favourably with type II neurones of Nambu & Llinas (1994).

The somata size of these two populations was also comparable, 20 × 11 μm (this study) and the 29 × 17 μm (Nambu & Llinas, 1997). These discrepancies may be due to differences in histological processing. Indeed, the size of the cell bodies and beaded dendrites of type A cells are features previously described in the majority of 'typical' GP cells (Fox *et al.* 1974; Difiglia *et al.* 1982; Millhouse, 1986; Park *et al.* 1992; Kita & Kitai, 1994).

Type B cells. Spontaneous action potential firing at rest, the lack of anomalous rectification (I_h), lack of rebound depolarisations and a lack of a mAHP primarily distinguish

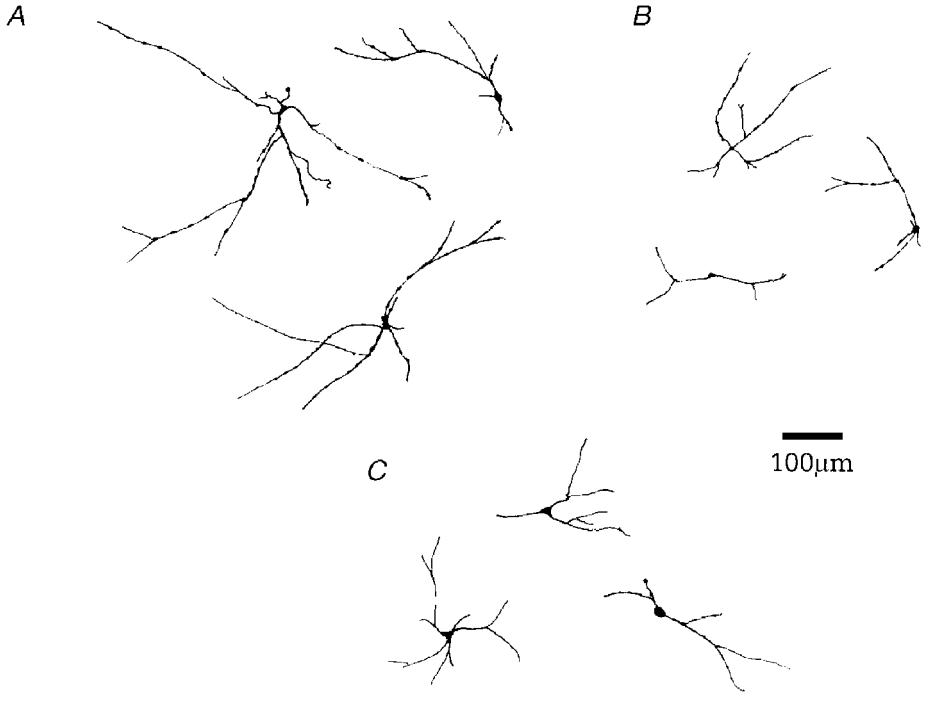

Figure 8. Morphological reconstruction of biocytin-labelled neurones

Of the 61 cells that were sufficiently well labelled with biocytin, 40 have been fully characterised electrophysiologically. *A*, examples of large multipolar type A neurones with extensive dendritic branching, which were mainly varicose (21/26 cells). *B*, representative examples of small oval type B GP cells whose dendrites were predominantly varicose (7/10 cells). *C*, examples of large pyramidal type C cells with extensive dendritic trees.

type B cells in this study. Statistical analysis of membrane properties highlighted a low input resistance and short membrane time constant. Upon current injection, these cells fired in an irregular pattern often in clusters of short duration action potentials with weak spike frequency adaptation. These features show similarities with the phasic cells described by Kita & Kitai (1991) constituting 18% of their GP population (32% in our study). No correlates were found with the studies of Nambu & Llinas (1994, 1997).

Type B cells were the smallest cells encountered (15·5 × 10·5 μm) with low-density dendritic arborisations. Indeed, small round cells with short varicose dendrites have been described in Golgi studies (Fox *et al.* 1974; Difiglia *et al.* 1982; Millhouse, 1986) and have been previously assumed to be interneurones. Further studies are required to verify whether type B cells are projection cells or true interneurones.

Type C cells. Although type C cells show some similarities to type I cells of Nambu & Llinas including the largest soma size (28 × 15 μm *versus* 40 × 23 μm) and resting membrane potential (−66 *versus* −65 mV), they do not appear to be the same as they were found on such an infrequent basis (5 *versus* 59%). These cells may well correspond to the two quiescent cells recorded by Kita & Kitai (1991) (9% of the

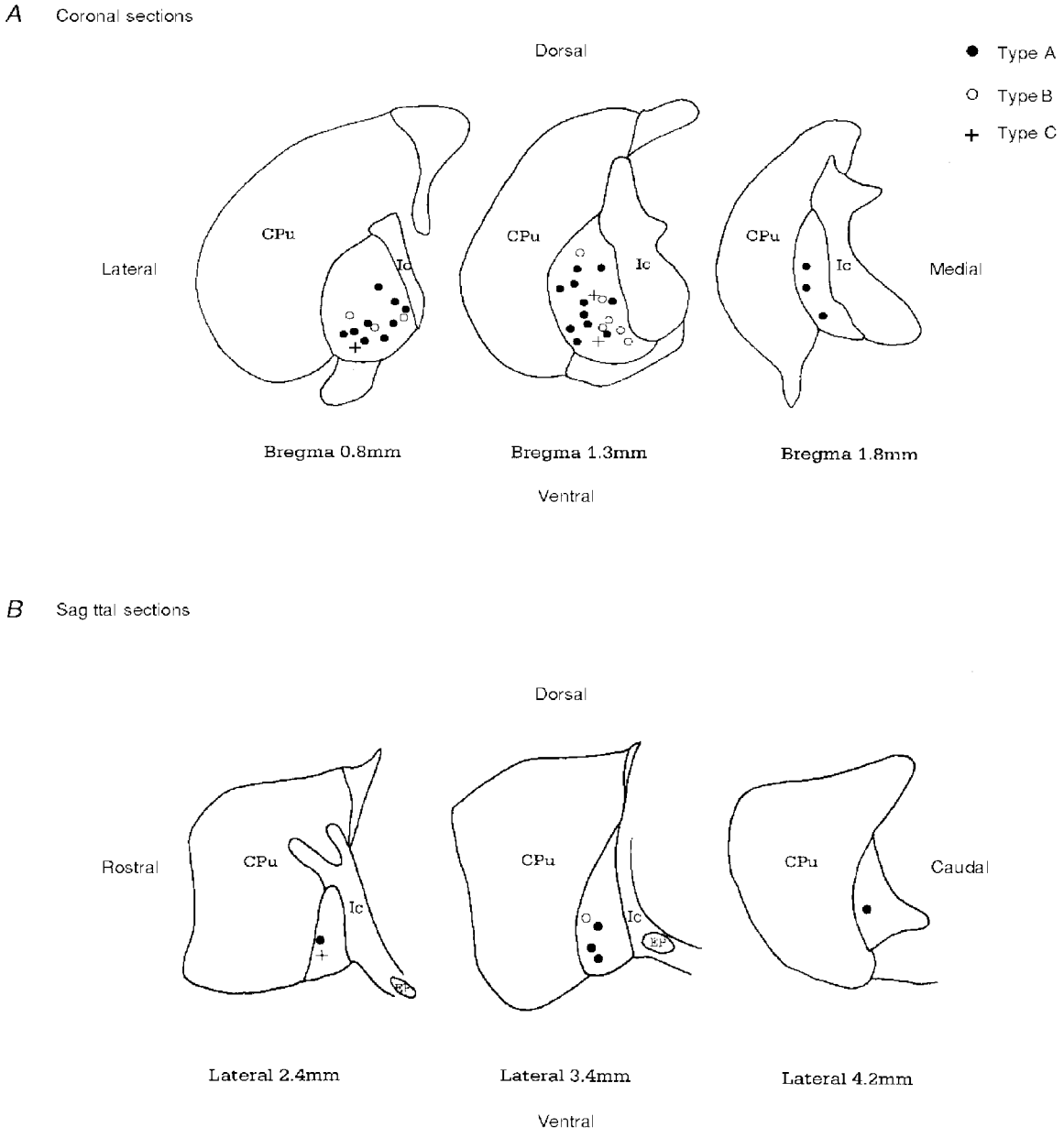

Figure 9. Topography of GP cells

The location of each biocytin-filled GP neurone was plotted onto stylised drawings of coronal (*A*) and sagittal (*B*) slices (obtained from Paxinos & Watson 1986). There appears to be a homogenous distribution of neuronal types A, B and C throughout the GP.

population) which exhibited long duration action potentials. Type C cells do exhibit ramp-like depolarisations on current injection which induced a gradual increase in action potential firing rate to a maximum of around 300 Hz. This ramp could be due to the inactivation of the large transient outward A-like potassium current observed in these cells. Indeed, type C neurones may correlate with the small population of GP cells found expressing a transient potassium current of the Kv3.4 family (Hernández-Pineda *et al.* 1999).

Although type C cells show no topographic distribution, this small population of quiescent neurones, which have a slightly larger soma than type A GP cells, may correspond to the cholinergic neurones previously found located along the medial lateral and ventral borders (Ingham *et al.* 1985) thought to be displaced cells from the basal nucleus of Meynert (Armstrong *et al.* 1983; Tkatch *et al.* 1998).

Topographical distribution

There appears to be little evidence for the topographical distribution of electrophysiologically classified GP neurones to match the pronounced topographical distribution of parvalbumin positive and negative neurones in the GP (Hontanilla *et al.* 1994; Rajakumar *et al.* 1994). On the other hand, the presence of four GP neuronal subtypes classified on the basis of calcium binding proteins (A. J. Cooper, unpublished observations) warrants further investigation.

Other cell types encountered

Two recordings and reconstruction of biocytin fills have been made of cells with a characteristic fusiform shape that appear to lie parallel to the striatal–GP border in coronal and sagittal slices. These cells may correspond to the border cells reported in *in vivo* studies (Delong, 1971) and the calbindin D-28k positive cells of similar form and location (A. J. Cooper, unpublished observations). Other subtypes of cells which were encountered included medium spiny striatal neurones with characteristic morphology, low resting membrane potential (< -75 mV), long AP duration (> 2 ms) and pronounced inward rectification (Kita *et al.* 1984; Kawaguchi *et al.* 1989), cells with classical characteristics of large striatal cholinergic interneurones (Kawaguchi, 1993) and neurones located in ventral areas of the pallidum, with large rebound depolarisations giving rise to bursts of 5 or 6 action potentials, were encountered. These latter cells may well correspond to type C neurones of the ventral pallidum (Lavin & Grace, 1996). No putative GP interneurones, type III cells of Nambu & Llinas (1994, 1997), were encountered. These may well have been displaced medium spiny striatal cells, a possibility acknowledged by these authors (Nambu & Llinás, 1994).

Activity-dependent characteristics

Although a major proportion of GP cells *in vitro* appear quiescent, the rate and pattern of firing in response to current injection shows clear differences between subtypes. The maximum firing frequency was greatest for B-type cells, while C-type cells could only sustain firing at a relatively low rate before spike-frequency accommodation and a failure of spike repolarisation.

Spike-frequency adaptation, a consequence of the calcium-activated slow I_{AHP} activation (Sah, 1996) was relatively weak in A- and B-type cells and masked in C-type cells by ramp depolarisation. However, the degree of adaptation rose on increasing current-step amplitude and firing frequency, presumably as a consequence of the increased intracellular calcium load. However, the degree of adaptation observed was undoubtedly compromised by the high concentration of the calcium chelator BAPTA (10 mM) that was used in the recording pipette. Indeed, spike frequency adaptation and train AHPs are enhanced if 1 mM EGTA is used as the internal calcium chelator (I. M. Stanford, unpublished observations).

The time course of AHPs following a single action potential appear to differentiate B-type cells from the other types. Both A- and C-type cells possess a medium AHP most likely due to the activation of the small conductance SK_{ca} potassium channels (Sah, 1996). However, the fast time course of the AHP in type B cells indicates that this channel is lacking in this neuronal population. This could be one of the factors that allows type B cells to fire at a faster rate in high frequency clusters.

All GP cell types possess a fast AHP (which may be blocked by TEA-Cl at 1 mM; I. M. Stanford, unpublished observations). This AHP may be due to either large conductance BK_{Ca} potassium channels (alternatively termed I_c) (Sah, 1996) or arise from the expression of the voltage-gated TEA-sensitive delayed rectifier Kv3.1 and Kv3.2 proteins (Baranauskas *et al.* 1999). These proteins have been found in abundance in parvalbumin positive GP cells (Hernández-Pineda *et al.* 1999) and have previously been associated with fast spiking cells with short duration action potentials such as the interneurones of the hippocampus and cortex (Kawaguchi, 1995; Du *et al.* 1996; Erisir *et al.* 1999).

Functional considerations

Both A- and B-type GP neurones are able to fire at very fast frequencies in excess of 350 Hz. Although, B-type cells fire in irregular clusters, no profound bursting activity was observed *in vitro*, in either cell type. However, type A cells do possess the currents I_h and I_t, and therefore appear well equipped to discharge at high frequencies in burst mode (Huguenard & McCormick, 1992). Indeed, following insults with the neurotoxin MPTP and subsequent depletion of dopamine, GP neurones *in vivo* have a tendency to burst fire with an increase in synchronous activity (Filion & Tremblay, 1991; Nini *et al.* 1995). This activity of the GP appears to be a fundamental requirement for the recruitment of the STN in such activity via rebound excitation (Plenz *et al.* 1999), also involving the currents I_h and I_t. This pacemaker activity is then entrained in the output nuclei of the basal ganglia, and may be responsible for the activity at the frequency of Parkinsonian tremor (Wichmann & DeLong,

1996; Bergman *et al.* 1998). Thus, in pathological conditions, GP cells may play a central role in the breakdown of independent neuronal activity and parallel processing required for normal function, the disruption of which leads to abnormal and pathological disorders of movement.

Summary

Based on whole-cell recordings and morphological data, two major and one minor population of neurones have been characterised from the GP of adult rats *in vitro*. These data represent a baseline for further studies on the functional role of the GP subtypes, which will be dependent on their projection fields, the integration of synaptic inputs, and the extent of local collateralisation and differential pharmacology.

Armstrong, D. M., Saper, C. B., Levey, A. I., Wainer, B. H. & Terry, R. D. (1983). Distribution of cholinergic neurons in rat brain: demonstrated by the immunocytochemical localization of choline acetyltranferase. *Journal of Comparative Neurology* **216**, 53–68.

Baranauskas, G., Tkatch, T. & Surmeier, D. J. (1999). Delayed rectifier currents in rat globus pallidus neurons are attributable to Kv2.1 and Kv3.1/3.2 K^+ channels. *Journal of Neuroscience* **19**, 6394–6404.

Bergman, H., Feingold, A., Nini, A., Raz, A., Slovin, H., Abeles, M. & Vaadia, E. (1998). Physiological aspects of information processing in the basal ganglia of normal and Parkinsonian primates. *Trends in Neurosciences* **21**, 32–38.

Bevan, M. D., Booth, P. A. C., Eaton, S. A. & Bolam, J. P. (1998). Selective innervation of neostriatal interneurons by a subclass of neuron in the globus pallidus. *Journal of Neuroscience* **18**, 9438–9452.

Bolam, J. P. & Smith, Y. (1992). The striatum and globus pallidus send convergent synaptic inputs onto single cells in the entopeduncular nucleus of the rat: a double antereograde labelling study combined with post-embedding immunocytochemistry for GABA. *Journal of Comparative Neurology* **321**, 456–476.

Cooper, A. J. & Stanford I. M. (2000) Dopamine-mediated presynaptic inhibition of striatal $GABA_A$ IPSCs in the rat globus pallidus *in vitro*. *Journal of Physiology* **525.P**, 52–53*P*.

Cornwall, J., Cooper, J. D. & Phillipson, O. T. (1990). Projections to the rostral reticular thalamic nucleus in the rat. *Experimental Brain Research* **80**, 157–171.

Delong, M. R. (1971). Activity of pallidal neurons during movement. *Journal of Neurophysiology* **34**, 414–427.

Difiglia, M., Pasik, P. & Pasik, T. (1982). A Golgi and ultrastructural study of the monkey globus pallidus. *Journal of Comparative Neurology* **212**, 53–75.

Du, J., Zhang, L., Weiser, M., Rudy, B. & McBain, C. J. (1996). Developmental expression and functional characterization of the potassium subunit Kv3.1b in parvalbumin-containing interneurons of the rat hippocampus. *Journal of Neuroscience* **16**, 506–518.

Erisir, A., Lau, D., Rudy, B. & Leonard, C. S. (1999). Function of specific K^+ channels in sustained high-frequency firing of fast-spiking neocortical interneurons. *Journal of Neurophysiology* **82**, 2476–2489.

Filion, M. & Tremblay, L. (1991). Abnormal spontaneous activity of globus pallidus neurons in monkeys with MPTP-induced parkinsonism. *Brain Research* **547**, 142–151.

Fox, C. A., Andrade, A. N., Luqui, I. J. & Rafols, J. A. (1974). The primate globus pallidus: A Golgi and electron microscopic study. *Journal fur Hirnforschung* **15**, 75–93.

Gandia, J. A., Delasheras, S., Garcia, M. & Giménez-Amaya, J. M. (1993). Afferent projections to the reticular thalamic nucleus from the globus pallidus and substantia nigra of the rat. *Brain Research Bulletin* **32**, 351–358.

Harris, N. C. & Constanti, A. (1995). Mechanism of block by ZD 7288 of the hyperpolarization-activated inward rectifying current in guinea pig substantia nigra neurons *in vitro*. *Journal of Neurophysiology* **74**, 2366–2378.

Hazrati, L. N. & Parent, A. (1991). Projections from the external pallidum to the reticular thalamic nucleus in the squirrel monkey. *Brain Research* **550**, 142–146.

Hernandez-Pineda, R., Chow, A., Amarillo, Y., Moreno, H., Saganich, M., De Miera, E. V. S., Hernandez-Cruz, A. & Rudy, B. (1999). Kv3.1–Kv3.2 channels underlie a high-voltage-activating component of the delayed rectifier K^+ current in projecting neurons from the globus pallidus. *Journal of Neurophysiology* **82**, 1512–1528.

Hontanilla, B., Parent, A. & Giménez-Samaya, J. M. (1994). Compartmental distribution of parvalbumin and calbindin D-28k in rat globus pallidus. *NeuroReport* **5**, 2269–2272.

Huguenard, J. R. & McCormick, D. A. (1992). Simulation of the currents involved in rhythmic oscillations in thalamic relay neurons. *Journal of Neurophysiology* **68**, 1373–1383.

Ingham, C. A., Bolam, J. P., Wainer, B. H. & Smith, A. D. (1985). A correlated light and electron microscopic study of identified cholinergic basal forebrain neurons that project to the cortex in the rat. *Journal of Comparative Neurology* **239**, 176–192.

Kawaguchi, Y. (1993). Physiological, morphological, and histochemical characterization of three classes of interneurons in rat neostriatum. *Journal of Neuroscience* **13**, 4908–4923.

Kawaguchi, Y. (1995). Physiological subgroups of non-pyramidal cells with specific morphological characteristics in layer II/III of rat frontal cortex. *Journal of Neuroscience* **15**, 2638–2655.

Kawaguchi, Y., Wilson, C. J. & Emson, P. C. (1989). Intracellular recording of identified neostriatal patch and matrix spiny cells in a slice preparation preserving cortical inputs. *Journal of Neurophysiology* **62**, 1052–1068.

Kincaid, A. E., Penny, J. B. Jr, Young, A. B. & Neumans, S. W. (1991). Evidence for a projection from the globus pallidus to entopeduncular nucleus in the rat. *Neuroscience Letters* **128**, 121–125.

Kita, H., Kita, T. & Kitai, S. T. (1984). Passive electrical membrane properties of rat neostriatal neurons in an *in vitro* slice preparation. *Brain Research* **300**, 129–139.

Kita, H. & Kitai, S. T. (1991). Intracellular study of rat globus pallidus neurons: membrane properties and responses to neostriatal, subthalamic and nigral stimulation. *Brain Research* **564**, 296–305.

Kita, H. & Kitai, S. T. (1994). The morphology of globus pallidus projection neurons in the rat: an intracellular staining study. *Brain Research* **636**, 308–319.

Lavin, A. & Grace, A. A. (1996). Physiological properties of rat ventral pallidal neurons recorded intracellularly *in vivo*. *Journal of Neurophysiology* **75**, 1432–1443.

Magill, P. J., Bolam, J. P. & Bevan, M. D. (2000). Relationship of activity in the subthalamic nucleus-globus pallidus network to cortical electroencephalogram. *Journal of Neuroscience* **20**, 820–833.

Millhouse, O. E. (1986). Pallidal neurons in the rat. *Journal of Comparative Neurology* **254**, 209–227.

Nambu, A. & Llinas, R. (1994). Electrophysiology of globus pallidus neurons *in vitro*. *Journal of Neurophysiology* **72**, 1127–1139.

Nambu, A. & Llinas, R. (1997). Morphology of globus pallidus neurons: Its correlation with electrophysiology in guinea pig brain slices. *Journal of Comparative Neurology* **377**, 85–94.

Nini, A., Feingold, A., Slovin, H. & Bergman, H. (1995). Neurons in the globus pallidus do not show correlated activity in the normal monkey, but phase-locked oscillations appear in the MPTP model of Parkinsonism. *Journal of Neurophysiology* **74**, 1800–1805.

Parent, A. & Hazrati, L.-N. (1995). Functional anatomy of the basal ganglia. II. The place of subthalamic nucleus and external pallidum in basal ganglia circuitry. *Brain Research Reviews* **20**, 128–154.

Park, M. R., Falls, W. M. & Kitai, S. T. (1992). An intracellular HRP study of the rat globus pallidus. I Responses and light microscopic analysis. *Journal of Comparative Neurology* **211**, 284–294.

Paxinos, G. & Watson, C. (1986). *The Rat Brain in Stereotactic Coordinates*. Academic Press, Sydney.

Plenz, D., Kitai, S. T. & Kital, S. T. (1999). A basal ganglia pacemaker formed by the subthalamic nucleus and external globus pallidus. *Nature* **400**, 677–682.

Rajakumar, N., Rushlow, W., Naus, C. C. G., Elisevich, K. & Flumerfelt, B. A. (1994). Neurochemical compartmentalization of the globus pallidus in the rat: an immunocytochemical study of calcium-binding proteins. *Journal of Comparative Neurology* **346**, 337–348.

Sah, P. (1996). Ca^{2+}-activated K^+ currents in neurones: types, physiological roles and modulation. *Trends in Neurosciences* **19**, 150–154.

Smith, Y. & Bolam, J. P. (1989). Neurons of the substantia nigra reticulata receive a dense GABA-containing input from the globus pallidus in the rat. *Brain Research* **493**, 160–167.

Smith, Y., Bolam, J. P. & von Krosigk, M. (1990). Topographical and synaptic organisation of GABA containing pallidosubthalamic projection in the rat. *European Journal of Neuroscience* **2**, 500–511.

Stanford, I. M. & Cooper, A. J. (1999). Presynaptic μ and δ opioid receptor modulation of $GABA_A$ IPSCs in the rat globus pallidus *in vitro*. *Journal of Neuroscience* **19**, 4796–4803.

Stanford, I. M. & Cooper, A. J (2000). Electrophysiological and morphological characterisation of rat globus pallidus neurones *in vitro*. *Journal of Physiology* **525.P**, 52*P*.

Stuart, G. J., Dodt, H. U. & Sakmann, B. (1993). Patch-clamp recordings from the soma and dendrites of neurons in brain slices using infrared video microscopy. *Pflügers Archiv* **423**, 511–518.

Tkatch, T., Baranauskas, G. & Surmeier, D. J. (1998). Basal forebrain neurons adjacent to the globus pallidus co-express GABAergic and cholinergic marker mRNAs. *NeuroReport* **9**, 1935–1939.

Wichmann, T. & Delong, M. (1996). Functional and pathophysiological models of the basal ganglia. *Current Opinion in Neurobiology* **6**, 751–758.

Corresponding author

I. M. Stanford: Department of Pharmacology, Division of Neuroscience, The Medical School, University of Birmingham, Edgbaston, Birmingham B15 2TT, UK.

Email: i.m.stanford@bham.ac.uk